JES Focus Issue on Progress in Molten Salts and Ionic Liquids

Electrochemical Reduction of UO_2 to U in LiCl-KCl Molten Salt Eutectic Using the Fluidized Cathode Process

Rema Abdulaziz,[a] Leon Brown,[a] Douglas Inman,[a] Clint A. Sharrad,[b] Arfon Jones,[c] Paul R. Shearing,[a] and Daniel J. L. Brett[a,z]

[a]*Electrochemical Innovation Lab, Department of Chemical Engineering, University College London, Torrington Place, London WC1E 7JE, United Kingdom*
[b]*School of Chemical Engineering and Analytical Science, University of Manchester, Manchester M13 9PL, United Kingdom*
[c]*Fissile Material Technology, AWE, Aldermaston RG7 4PR, United Kingdom*

The electrochemical reduction of UO_2 to U metal has been investigated in both Fluidized Cathode (FC) and Metallic Cavity Electrode (MCE) cell arrangements. Differences in the local concentration of O^{2-} where the reduction takes place influnces the reduction potential. The fleeting contact of UO_2 particle contact with the current collector in case of the FC results in much less O^{2-} buildup compared to MCE. Consequently, UO_2 reduction occurs over a range of potentials in the FC and may involve separate two 2-electron steps compared to one apparent 4-electron step in the MCE. It is proposed that there are three discrete periods during the FC reduction process. The first is an induction period during which reduced uranium particles gradually adhere to the tungsten current collector. The second is reduction associated with a rapid growth in electrode area and consequent increase in current. The third is a slower reduction of the remaining oxide in the melt. Complete reduction of metallic U is achieved at −2.2 V (vs. Ag/Ag^+) with an estimated faradaic current efficiency of >92%.
 [DOI: 10.1149/2.0421708jes]

Manuscript submitted February 8, 2017; revised manuscript received June 19, 2017. Published July 5, 2017. This was Paper 3450 presented at the Honolulu, Hawaii, Meeting of the Society, October 2–7, 2016. *This paper is part of the JES Focus Issue on Progress in Molten Salts and Ionic Liquids.*

There are significant drivers for pursuing the next generation of nuclear reactors. Generation IV reactors offer both advancements in reactor design and also feature fully integrated fuel reprocessing capabilities. There are six types of Generation IV nuclear reactors and power plants under development. These are: the very-high-temperature reactor (VHTR), the sodium-cooled fast reactor (SFR), the supercritical-water-cooled reactor (SCWR), the gas-cooled fast reactor (GFR), the lead-cooled fast reactor (LFR), and the molten salt reactor (MSR). The key features of each are summarized in Table I. The fuel type used in the majority of these reactors is metal. Given that most current reactors employ metal oxide (MOX or UOX) fuel and the majority of legacy waste is also metal oxide, the conversion of metal oxides to metals is an important component in a future nuclear power flow sheet.

High temperature molten salt reprocessing technology (pyroprocessing)[2] for spent nuclear fuel offers a range of advantages when compared to aqueous reprocessing techniques. This is due to: an improved proliferation resistance (local processing reduces the likelihood of material diversion, no separation of plutonium); using facilities with a smaller footprint; a shorter cooling period for irradiated fuel, and also improved criticality safety margins. Different process systems and salts have been studied in pyroprocessing, most of which are summarized by the Nuclear Energy Agency (NEA).[3]

Conceptual flow sheets for the pyrochemical treatment of used nuclear fuel are described by Argonne National Lab (ANL).[4] The spent nuclear fuel, in the form of oxide pellets, is decladded and chopped, then passed on for an electrolytic reduction step. The uranium is in the form of UO_2; hence, the reduction of UO_2 to U metal is being investigated here. The reduced species then undergo electrorefining,[5–9] where U product and other transuranic species are separated and recycled into new fuel.

Studies of spent fuel oxides in molten salts have identified two possible reaction pathways, differing reduction potentials and varying distribution of residual oxide in the product. In a study by Hermann et al.,[10] crushed spent fuel was loaded into a stainless steel basket and submerged in molten LiCl-1 wt% Li_2O at 650°C. A platinum anode and a Ni/NiO reference electrode were used. They determined that direct electrochemical reduction occurred at −2.40 V (vs. Ni/NiO) (Equation 1), and that Li deposition occurred at −2.47 V (vs. Ni/NiO) (Equation 2). The potential difference of only 70 mV between the two reactions meant that maintaining exclusively direct electro-reduction was difficult and that chemical reduction also took place with Li formed by reduction of the electrolyte (Equation 3).

$$UO_2 \leftrightarrow U + O_2 \quad \text{Direct Reduction Pathway} \qquad [1]$$

$$Li_2O \leftrightarrow 2Li + \frac{1}{2}O_2 \quad \text{Electrolysis of the Melt} \qquad [2]$$

$$4Li + UO_2 \leftrightarrow U + 2Li_2O \quad \text{Indirect/Chemical Reduction Pathway} \qquad [3]$$

In contrast, Hur et al.[11] carried out the reduction of UO_2 to U metal in molten LiCl-KCl-Li_2O at 520°C. The reduction potential was at −1.27 V (vs. Li-Pd). They established that the reduction process was entirely via the indirect/chemical reduction pathway.

The influence of varying oxide particle size has also been examined. Choi et al.[12] reduced 17 kg of UO_2 to U metal in LiCl-Li_2O. They concluded that a small pellet size, with a high anode surface area resulted in higher current efficiencies.

Similar conclusions were drawn by Jeong et al.[13] during which greater than 99% of 20 kg of U_3O_8 were successfully reduced at potentials ranging from −2.47 V to −3.46 V (vs. Pt). The authors concluded that increasing in the size of the oxide pellets inhibited the penetration of electrolyte and thus led to an unreduced core. This can be explained by the three-phase interline (3PI) theory.[14–16] Seo et al.[17] determined the main reduction potential for reducing U_3O_8 to U to be −2.27 V (vs. Pt).

Sakamura et al.[18] compared the reduction of UO_2 in both $CaCl_2$ and LiCl. The reduction in $CaCl_2$ appeared at < 0.6 V (vs. Ca/Ca^{2+}) at 800°C. and in LiCl the reduction potential was < 0.15 V (vs. Li/Li^+) at 650°C. Reduction in LiCl exhibited a higher current efficiency and superior apparent electrolyte penetration into the oxide particles. The reduction potentials in both systems were established to be very

[z]E-mail: d.brett@ucl.ac.uk

Table I. Generation IV reactor designs under development.[1]

Reactor	Neutron spectrum	Coolant	Temperature°C	Fuel cycle	Fuel type	Size (MW_e)
VHTR	Thermal	Helium	900 – 1000	Open	Oxide	100–300
SFR	Fast	Sodium	550	Closed	Metal/oxide	50–1500
SCWR	Thermal/fast	Water	510 – 625	Open/closed	Oxide	1000–1600
GFR	Fast	Helium	850	Closed	Metal	1000
LFR	Fast	Lead	480 – 800	Closed	Metal	20–1200
MSR	Fast/thermal	Fluoride salts	700 – 800	Closed	Metal*	1000

*The metal is dissolved in the fluoride salt (e.g. UF_4 and ThF_4).

close to the salts' decomposition potentials. In all of these studies, the reduction of UO_2 to U metal appeared to take place without any intermediate uranium oxide being formed, e.g. UO.[19]

The differing behaviors found in these studies may be attributed to the varying activity of O^{2-} ions in the melt. When the metal oxide's reduction potential and the salt's decomposition potential approach one another, as is the case for the reduction of UO_2, this has a substantial influence upon the reaction pathway of the process.

The fluidized cathode (FC) process[20,21] is a metal oxide to metal reduction process where the oxide particles are suspended in the molten salt and fluidized to impinge on the current collector to be reduced. A 3PI is created each time a metal oxide particle comes into contact with the current collector. The continuous agitation of the fluidized cathode enhances the mixing of electrolyte and metal oxide particles, and the transport of oxygen ions within the electrolyte. In this article, the electrochemical reduction of UO_2 to U metal in LiCl-KCl molten salt eutectic is investigated, using both metallic cavity electrodes (MCEs)[22–25] and the fluidized cathode (FC) arrangements. Observations on the reduction pathways and the current efficiency are reported.

Experimental

Apparatus.—A schematic of the electrolytic cell used is given in Fig. 1a. The cathode consists of a pure tungsten rod current collector immersed in the molten salt (LiCl-KCl) eutectic containing suspended UO_2 particles. The melt is agitated via a flow of argon. The tungsten rod has a glass sheath so that 4 cm is exposed to the salt.

The anode is a graphite rod contained in its own compartment to avoid reoxidation of the reduced uranium particles. A reference electrode (Ag/Ag^+) is also used. The temperature was monitored via a thermocouple immersed in the melt. All electrochemical tests were performed using a potentiostat (IviumStat, Ivium Technologies, NL).

A broadly similar arrangement was used to carry out the metallic cavity electrode (MCE) experiments with the UO_2 particles confined to the cavity and not suspended in the melt. This is illustrated in Fig. 1b. The cavities in the MCE were filled with UO_2 powder. The same powder used for the fluidized cathode experiments. The MCEs were made using a 0.5 mm thick molybdenum sheet (Sigma-Aldrich, 99.9% purity). The sheet was cut into 5 mm wide and 6 cm long strips. Holes, or cavities, of 0.4 mm diameter were drilled at one end of the strips. These strips were then attached to a tungsten rod using a molybdenum wire. When experiments were run, it was ensured that only half of a strip was immersed in the molten salt, with all the cavities exposed to the electrolyte, but keeping the wire and the tungsten rod above it.

Chemicals.—All preparation steps were carried out under a sealed argon atmosphere. Anhydrous lithium chloride (ACS reagent, ≥99.0% purity, Sigma-Aldrich) and potassium chloride (≥99.5% purity, Sigma-Aldrich) were used for the electrolyte. The salt was dried in a vacuum oven at 200°C for 24 h, then 150 g of 59–41 mol% LiCl-KCl were mixed with UO_2 (as received from the Centre for Radiochemistry Research, School of Chemistry, University of Manchester). The X-ray diffraction pattern of the as-received UO_2 powder can be found in supplemental material (S1). 15 g of LiCl-KCl was placed inside the anode compartment. The counter electrode was a high density graphite rod, 3.05 mm in diameter (99.9995% metal basis, Alfa Aesar). The working electrode (current collector) was a tungsten rod, 1.5 mm in diameter (99.95% metal basis, Alfa Aesar). A glass sheath around the shaft of the tungsten rod insured that a constant surface area of electrode is exposed to the electrolyte, even when being agitated by the Ar stream. Argon (99.998% purity, BOC) was bubbled through the melt via a ceramic tube (5 mm internal diameter, Alsint).

For the MCE experiments, the electrolyte was composed of 150 g of LiCl-KCl, prepared in the same way as for the fluidized cathode setup, but no UO_2 particles were agitated in the melt. The

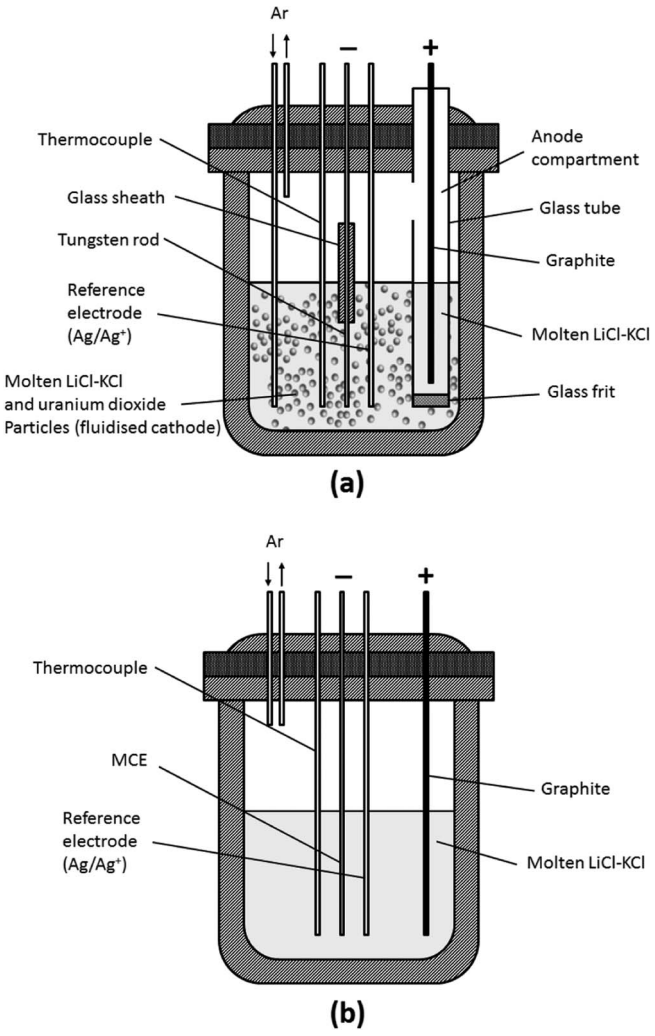

Figure 1. Electrolytic cells; (a) for the electrochemical reduction of metal oxide powder using the fluidized cathode method; (b) for the electrochemical reduction of metal cavity electrodes (MCEs).

Table II. Gibbs energy of formation for species in the Li-K-U-O-Cl system at 500°C.

Species	ΔG_f^0 (kJ mol^{-1}) at 500°C	Comments	References
LiCl	−344.887		31–33
Li_2O	−498.105		31, 34–38
KCl	−362.418		39, 40
K_2O	−255.559		34, 35
Li_2UO_4	−1662.680	Extrapolated above 27°C	37, 38, 41
UO	−477.980	Extrapolated above 227°C	42
UO_2	−950.563		35, 43
U_4O_9	−3921.203		35
U_3O_8	−3055.659		35
UO_3	−1023.699		31, 34, 35
UCl_2O	−888.723		36, 41
$U_2Cl_5O_2$	−1796.568	Extrapolated above 427°C	37
UCl_3	−692.619		37, 41
UCl_4	−794.542		31, 44

cavities in the working electrode were filled with UO_2 powder by 'finger pressing' using two glass slides.

Procedure.—Experiments were carried out under a dry argon atmosphere at a melt temperature of 450°C. Argon was bubbled into the melt, which resulted in a homogeneous distribution of particles as assessed by visual inspection. A constant length of 4 cm (3.84 cm^2 initial surface area) of the current collector was immersed in the melt during the fluidized cathode measurements, and all the holes in the MCE, making sure that the Mo wire and W rod stayed outside the melt. Absolute currents are reported due to the fact that the electrode surface area changes during experiments.

Results and Discussion

A predominance diagram[26–29] was constructed for the Li-K-U-O-Cl system, relating the potential E vs. standard chlorine electrode (S.Cl.E) to the negative logarithm of O^{2-} ions activity, pO^{2-}. All the thermodynamic data used for the production of the diagram is presented in Table II. A predominance diagram for uranium species in LiCl-KCl has previously been published.[28,30] However, the diagram reported here utilises more recent thermodynamic data and a greater number of stable species.

Table III. Thermodynamically calculated values of pO^{2-} and potentials required for Equations 4 and 5 to take place.

Reaction	pO^{2-}	E (V vs. S.Cl.E)	E (V vs. Ag/Ag$^+$)
4	6.200 – 21.650	−3.558 – −2.374	−2.422 – −1.238
5	6.500 – 21.750	−3.562 – −2.394	−2.426 – −1.258

The predominance diagram in Fig. 2 shows the different regions of stability for different compounds and oxidation states of uranium. Thermodynamically, one can deduce that the concentration of O^{2-} ions in the eutectic melt greatly affects the reduction process of UO_2 to U metal. Starting with UO_2, two reduction reactions take place to produce U metal. These are presented in Equations 4 and 5. Equations 6 and 7 are used to calculate the potential, E, needed for each reaction to take place, at different values of O^{2-} ion activity.

$$UO_2 + 2e^- \leftrightarrow UO + O^{2-} \quad [4]$$

$$UO + 2e^- \leftrightarrow U + O^{2-} \quad [5]$$

$$E_4 = \frac{-\Delta G_4^0}{2F} + \frac{RTln10}{2F} pO^{2-} \quad [6]$$

$$E_5 = \frac{-\Delta G_5^0}{2F} + \frac{RTln10}{2F} pO^{2-} \quad [7]$$

The pO^{2-} ranges and potential bands (vs. S.Cl.E and Ag/Ag$^+$ references electrode) are presented in Table III for the reactions described in Equations 4 and 5.

Cyclic voltammetry measurements were performed on an MCE molybdenum electrode packed with UO_2 powder; this is presented in Fig. 3. It was scanned from 0 V to −2.5 V, and back to 0 V (vs. Ag/Ag$^+$). The coupled redox potentials at 1, 2, 1′ and 2′ represent the reduction of a thin film of oxide on the MCE molybdenum strip and its reoxidation. The redox pair A and A′ represent the reduction of UO_2 to U metal, and its reoxidation to UO_x, as shown in the overall reaction described in Equation 8. This is consistent with previous results.[19] The reduction potential appears to be very close to the salt's decomposition potential; hence, indicating a high O^{2-} ion activity.

$$UO_2 + 4e^- \leftrightarrow U + 2O^{2-} \quad [8]$$

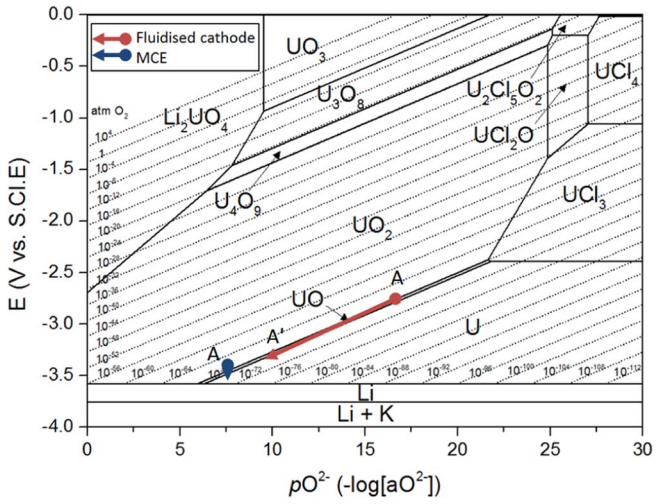

Figure 2. Predominance diagram for the Li-K-U-O-Cl system at 500°C. The red and blue lines show the voltage range over which the Fluidized Cathode and MCE reduction occurs tracked along the transition from UO_2 to U.

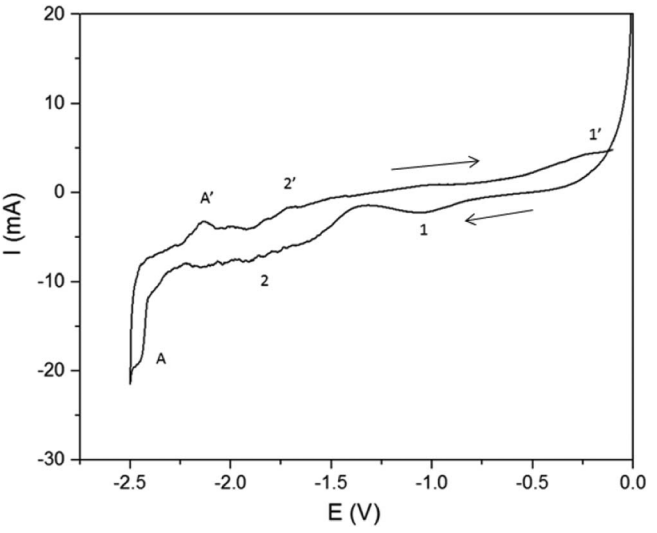

Figure 3. Cyclic voltammogram of UO_2 in molybdenum metallic cavity electrode (MCE) in LiCl-KCl eutectic at 450°C, scan rate: 20 mV s^{-1}, reference electrode: Ag/Ag$^+$.

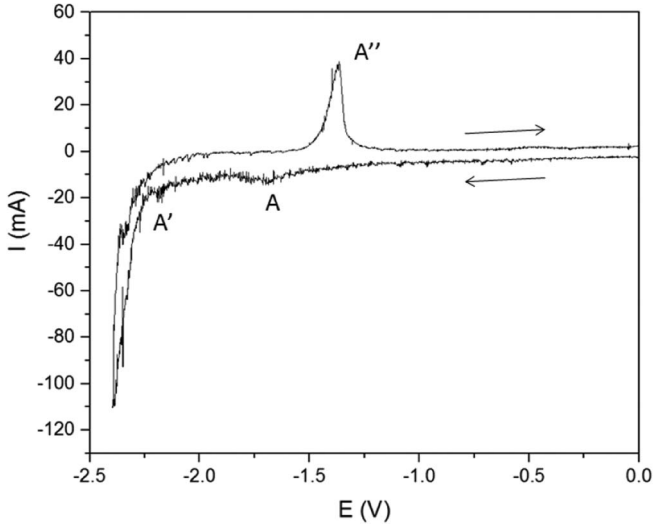

Figure 4. Cyclic voltammetry of UO_2 fluidized cathode (FC) in LiCl-KCl eutectic at 450°C, 5 g UO_2, argon flow rate: 600 cm^3 min^{-1}, reference electrode: Ag/Ag^+, Scan rate: 50 mV s^{-1}.

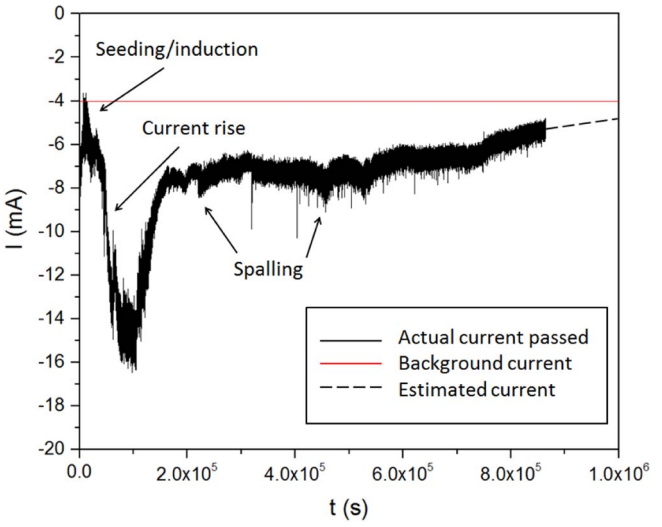

Figure 5. Chronoamperogram of UO_2 fluidized cathode in LiCl-KCl eutectic at 450°C, 4 g UO_2, argon flow rate: 600 cm^3 min^{-1}, set voltage: −2.2 V, reference electrode Ag/Ag^+.

Voltammetry measurements were performed on the FC arrangement, Fig. 4. It was scanned from 0 V to −2.4 V, and back to 0 V (vs. Ag/Ag^+). The current that passes between A and A′ represent the reduction of UO_2 to U metal. The peak at A″ represents the reoxidation of U to UO_x.

When comparing the voltammograms in Fig. 4 (FC) and Fig. 3 (MCE), one can see that peaks A and A′ occur earlier in the cathodic sweep with the FC (−1.7 V and −2.2 V) than the MCE (−2.4 V). In the FC process, a 3PI is initiated at the collision point of an oxide particle with the current collector and reaction extends from this point. When using an MCE, the 3PI is initially defined at the circumference of the packed metal oxide (where it meets the metal strip current collector and the salt) and there is a local buildup of oxide ions in the melt close to the 3PI (within the pores of the sample) as the reduction proceeds, thus compelling the reaction to take place at lower potentials than for the FC arrangement. When comparing the voltammetry of the MCE to previously published results using pellets,[18] one can see similarities in terms of the absence of the noise observed in the FC, and the reduction potential occurring very close to the salt decomposition potential.

Figure 4 indicates that the reduction starts at ∼ −1.7 V and extends to ∼ −2.2 V as the reduction process can be exposed to a broader range of pO^{2-} and may be a combination of two 2-electron transfer processes (Equations 4 and 5). The apparent 4-electron reaction found in the MCE might also be two 2-electron transfer processes, but close to one another. Previous studies[45,46] suggest that UO can exist in equilibrium in the presence of other uranium oxide states. Using the voltammetry information from Fig. 3 and Fig. 4, the possible reaction pathway for the reduction of UO_2 to U has been plotted on the predominance diagram in Fig. 2 showing both the potential (vs. S.Cl.E) and the O^{2-} ion activity, as the reaction proceeds. The activity of O^{2-} using the fluidized cathode process is lower and varies as the reaction proceeds, providing a larger potential range over which the reactions can occur, which allows more feasibility for a 2-electron transfer process.

To explore the reduction process with time, a constant potential of −2.2 V (vs. Ag/Ag^+) was applied to the fluidized cathode (containing 4 g of UO_2 powder), Fig. 5. As time passed, the current increased due to an increase in the electrode surface area and the deposit growth of U on the current collector surface. Another reason for the current increase could be the reduction in particle size distribution of the material due to some of it being reduced, thus enabling higher salt penetration and ultimately causing a higher reduction rate. When comparing the chronoamperogram to that for the reduction of tungsten oxide,[21] one can see that it takes a longer time for the electrode to start growing, observed as an increase in the current. It is possible that a 'seeding' effect exists whereby uranium metal takes some time to be deposited on the current collector. This is possibly due to the fact that the current collector is made from a different metal from that in the melt, compared with the all-tungsten system which did not exhibit this induction period. Formation of U on the W current collector is visible through the glass cell during the reduction process. At about 90,000 s, there is a rapid reduction in current associated with spalling off of the deposit from the electrode. New growth is then associated with the increase in the current, a similar characteristic of the process as seen in the reduction of WO_3.[20,21] A 'seeding' period is not observed after a spalling event suggesting that not all the reduced material falls off the electrode surface when this occurs.

Figure 6a shows an image of the current collector after the reduction has taken place. When the agitation is discontinued and the process is allowed to cool to room temperature, some metallic uranium metal accumulates at the bottom of the reaction vessel, Figs. 6b, 6c. Above that is black uranium oxide. Due to the similarity in appearance of U and UO_2, it was difficult to delineate the boundary between them in the figure. This stratification may be the basis of a separation method, as is the case with tungsten oxide reduction.

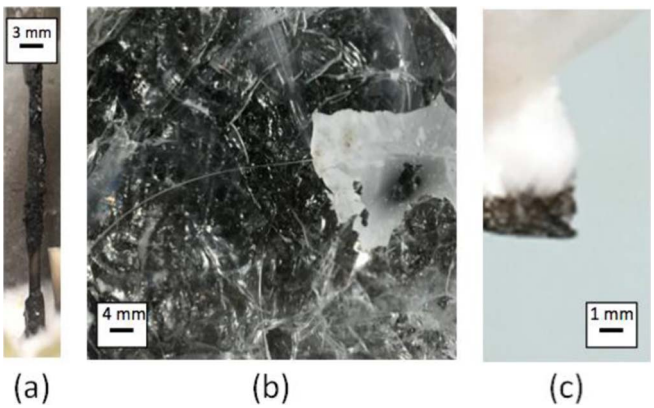

Figure 6. (a) Photograph of reduced uranium deposited on tungsten working electrode, (b) photograph of the bottom of the glass crucible showing the uranium product, (c) photograph of the solidified product, showing two separate layers of salt and uranium metal.

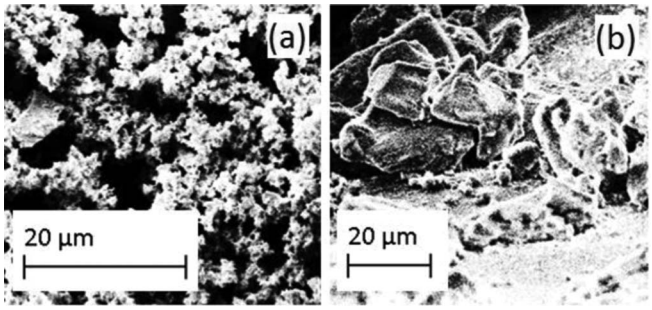

Figure 7. SEM images of (a) the as-received UO_2 particles, and (b) product U fused with some LiCl-KCl salt.

Figure 7. (a) shows an SEM image of the as-received UO_2 particles and (b) an SEM image of the U metal product from the solidified melt. The UO_2 powder has an average particle size of ∼1 µm, whereas the U product is in the form of agglomerated particles forming a larger particle size fused with some salt. Here, the use of vacuum distillation to separate the final product from the salt would be beneficial, as the salt could be melted and extracted from the metal product which possesses a much higher melting temperature.

Current efficiency.—To establish the current efficiency of the process, a constant potential of −2.2 V (vs. Ag/Ag^+) was applied to the fluidized cathode set-up to reduce 4 g of UO_2 to U metal, Fig. 5. The chronoamperogram shows a similar trend to previously published work on electrochemical reduction of metal oxides.[47]

Assuming 100% current efficiency, it would require a total of 5718 C to be applied to fully reduce all of the UO_2. The final product retrieved from the electrode's surface was analyzed via XRD (available in supplemental material, S2). The spectrum highlights features associated with KCl, and α-U. Most importantly, it shows that there is no sign of any uranium oxide species, namely UO_2 or UO. Thus, it confirms that complete conversion is possible at the electrode via the FC electrochemical process (in this case, unreacted oxide particles were in the solidified melt).

Calculating an accurate faradaic efficiency is challenging for such a system as it requires the process going to completion (which takes a long time) or having accurate measure of the product formed. Consideration of the background currents caused by trace oxygen in the system must also be made (this is taken to be 4 mA from pre-electrolysis measurements).

The product was separated from LiCl-KCl by repeated dissolution in ethanol under argon for 24 hours and vacuum drying (repeated three times). Despite this rigorous cleaning process, the XRD spectrum (refer to supplemental material, S2) confirms that KCl is remains present.

Instead, the faradaic efficiency of the process was calculated by dividing the theoretical charge required by the charge passed for a known mass of UO_2. To account for the background current and the process not going to completion, a faradaic efficiency range can be determined by linearly extrapolating the current to either background current as a limit of reaction or to zero. In which case, the process results in a current efficiency between 92% and 100%.

Conclusions

The electrochemical reduction of UO_2 to U metal has been investigated and found to depend on the method used (MCE or FC), with different local pO^{2-} in each case taken to be responsible. The MCE arrangement follows an apparent 4-electron transfer at a potential close to Li formation. The FC reduction occurs over a range of potentials and it is proposed that is taken to be due to the fleeting interactions of the particle with the current collector and good access of molten salt which results in lower pO^{2-} range and consequently less negative reduction potential. This may involve multiple electron transfer steps.

There are three periods during the FC reduction process at constant voltage. The first where a seeding process is thought to take place to allow for the reduced uranium particles to be deposited onto the tungsten current collector; the second where reduction of UO_2 particles occurs with a growth in electrode size accompanied by an increase in current being passed; the third where slower reduction of the remaining oxides in the melt occurs. The faradaic efficiency of the process has been estimated to be >92%.

The molten salt fluidized cathode is a robust, high-efficiency process for the electroreduction of metal oxides. It has been studied here for the electrochemical reduction of UO_2; however, it is likely applicable for other spent fuel oxides (such as UO_3 and PuO_2), and in the production of refractory metals, such as titanium. Separation of product from the melt as part of an industrial process could employ vacuum distillation at high temperature to remove the salt whilst still molten.[48,49]

Acknowledgments

This work was carried out as part of the UK Engineering and Physical Sciences Research Council (EPSRC) funded REFINE consortium (http://www.refine.eng.ed.ac.uk/) (EP/J000531/1) and EPSRC PACIFIC programme (EP/L018616/1). Shearing acknowledges financial support from the Royal Academy of Engineering and we acknowledge AWE for sponsoring molten salts research in the EIL. This article is dedicated to Professor Douglas Inman.

References

1. J. E. Kelly, *Progress in Nuclear Energy*, **77**, 240 (2014).
2. J. Laidler, J. Battles, W. Miller, J. Ackerman, and E. Carls, *Progress in Nuclear Energy*, **31**, 131 (1997).
3. NEA, Pyrochemical Separations in Nuclear Applications, (2004).
4. M. Williamson and J. Willit, *Nuclear Engineering and Technology*, **43**, 329 (2011).
5. J. Willit, W. Miller, and J. Battles, *Journal of Nuclear Materials*, **195**, 229 (1992).
6. Z. Tomczuk, J. P. Ackerman, R. D. Wolson, and W. E. Miller, *Journal of The Electrochemical Society*, **139**, 3523 (1992).
7. T. Koyama, M. Iizuka, Y. Shoji, R. Fujita, H. Tanaka, T. Kobayashi, and M. Tokiwai, *Journal of Nuclear Science and Technology*, **34**, 384 (1997).
8. Y. Sakamura, T. Hijikata, K. Kinoshita, T. Inoue, T. S. Storvick, C. L. Krueger, L. F. Grantham, S. P. Fusselman, D. L. Grimmett, and J. J. Roy, *Journal of Nuclear Science and Technology*, **35**, 49 (1998).
9. J. Roy, L. Grantham, D. Grimmett, S. Fusselman, C. Krueger, T. Storvick, T. Inoue, Y. Sakamura, and N. Takahashi, *Journal of the Electrochemical Society*, **143**, 2487 (1996).
10. S. Herrmann, S. Li, M. Simpson, and S. Phongikaroon, *Separation Science and Technology*, **41**, 1965 (2006).
11. J.-M. Hur, S.-S. Hong, and H. Lee, *J Radioanal Nucl Chem*, **295**, 851 (2013).
12. E.-Y. Choi, J.-M. Hur, I.-K. Choi, S. G. Kwon, D.-S. Kang, S. S. Hong, H.-S. Shin, M. A. Yoo, and S. M. Jeong, *Journal of Nuclear Materials*, **418**, 87 (2011).
13. S. M. Jeong, S. B. Park, S. S. Hong, C. S. Seo, and S. W. Park, *J Radioanal Nucl Chem*, **268**, 349 (2006).
14. G. Chen, E. Gordo, and D. Fray, *Metall and Materi Trans B*, **35**, 223 (2004).
15. Y. Deng, Wang, W. Xiao, Jin Hu, and G. Z. Chen, *The Journal of Physical Chemistry B*, **109**, 14043 (2005).
16. P. Kar and J. W. Evans, *Electrochimica Acta*, **54**, 835 (2008).
17. C. S. Seo, S. B. Park, B. H. Park, K. J. Jung, S. W. Park, and S. H. Kim, *Journal of Nuclear Science and Technology*, **43**, 587 (2006).
18. Y. Sakamura, M. Kurata, and T. Inoue, *Journal of The Electrochemical Society*, **153**, D31 (2006).
19. L. Brown, R. Abdulaziz, R. Jervis, V. Bharath, R. Attwood, C. Reinhard, L. Connor, S. Simons, D. Inman, and D. Brett, *Journal of Nuclear Materials*, **464**, 256 (2015).
20. R. Abdulaziz, L. D. Brown, D. Inman, S. Simons, P. R. Shearing, and D. J. L. Brett, *Electrochemistry Communications*, **41**, 44 (2014).
21. R. Abdulaziz, L. D. Brown, D. Inman, P. R. Shearing, and D. J. L. Brett, *Electrochimica Acta*, **226**, 18 (2017).
22. G. Qiu, M. Ma, D. Wang, X. Jin, X. Hu, and G. Z. Chen, *Journal of the Electrochemical Society*, **152**, E328 (2005).
23. G. Qiu, X. Feng, M. Liu, W. Tan, and F. Liu, *Electrochimica Acta*, **53**, 4074 (2008).
24. J. Peng, Y. Deng, D. Wang, X. Jin, and G. Z. Chen, *Journal of Electroanalytical Chemistry*, **627**, 28 (2009).
25. J. Peng, G. Li, H. Chen, D. Wang, X. Jin, and G. Z. Chen, *Journal of the Electrochemical Society*, **157**, F1 (2010).
26. R. Littlewood, *Journal of the Electrochemical Society*, **109**, 525 (1962).
27. K. Dring, R. Dashwood, and D. Inman, *Journal of the Electrochemical Society*, **152**, D184 (2005).
28. L. D. Brown, R. Abdulaziz, S. Simons, D. Inman, D. J. L. Brett, and P. R. Shearing, *Journal of Applied Electrochemistry*, **43**, 1235 (2013).

29. R. Abdulaziz, L. D. Brown, D. Inman, S. Simons, P. R. Shearing, and D. J. Brett, *Int. J. Electrochem. Sci*, **11**, 10417 (2016).
30. I. Uchida, J. Niikura, and S. Toshima, *Journal of electroanalytical chemistry and interfacial electrochemistry*, **124**, 165 (1981).
31. I. Barin, *Thermodynamical Data of Pure Substances*, VCH Verlags Gesellschaft, Weinheim (1993).
32. M. W. Chase, *JANAF thermochemical tables*, American Institute of Physics, New York (1985).
33. Landolt-Bornstein, *Thermodynamic Properties of Inorganic Materials*, Springer-Verlag, Berlin-Heidelberg (1999).
34. V. Glushko, *IVTAN Association, Izhorskaya*, **13**, 127412 (1994).
35. Landolt-Bornstein, *Thermodynamic Properties of Inorganic Materials*, Springer-Verlag, Berlin-Heidelberg (2001).
36. I. Barin, *Thermodynamical Data of Pure Substances*, VCH Verlags Gesellschaft, Weinheim (1989).
37. O. Knacke, O. Kubaschewski, and K. Hesselmann, Springer Verlag, Düsseldorf, Germany, 1 (1991).
38. M. Binnewies and E. Milke, *Thermochemical data of elements and compounds*, Wiley-VCH (2002).
39. D. G. Archera, *J. Phys. Chem. Ref. Data*, **28** (1999).
40. I. Barin, *Thermodynamical Data of Pure Substances*, VCH Verlags Gesellschaft, Weinheim (1995).
41. NEA, R. Guillaumont and F. J. Mompean, *Update on the Chemical Thermodynamics of Uranium, Neptunium, Plutonium, Americium and Technetium*, Elsevier (2003).
42. L. P. Ruzinov and B. S. Gulyanitskii, *Equilibrium Transformations of Metallurgical Reactions*, Moscow (1975).
43. I. Barin, *Thermodynamical Data of Pure Substances*, VCH Verlags Gesellschaft, Weinheim (1977).
44. Landolt-Bornstein, *Thermodynamic Properties of Inorganic Materials*, Springer-Verlag, Berlin-Heidelberg (2000).
45. S. Abramowitz, N. Acquista, and K. R. Thompson, *The Journal of Physical Chemistry*, **75**, 2283 (1971).
46. M. C. Heaven, J.-P. Nicolai, S. J. Riley, and E. K. Parks, *Chemical Physics Letters*, **119**, 229 (1985).
47. R. Bhagat, M. Jackson, D. Inman, and R. Dashwood, *Journal of the Electrochemical Society*, **155**, E63 (2008).
48. M. Rosenthal, P. Kasten, and R. Briggs, *Nuclear Technology*, **8**, 107 (1970).
49. M. J. Earle, J. M. Esperança, M. A. Gilea, J. N. C. Lopes, L. P. Rebelo, J. W. Magee, K. R. Seddon, and J. A. Widegren, *Nature*, **439**, 831 (2006).